p110γ deficiency protects against pancreatic carcinogenesis yet predisposes to diet-induced hepatotoxicity

Carolina Torres[a,1], Georgina Mancinelli[a], Jose Cordoba-Chacon[b], Navin Viswakarma[c,d], Karla Castellanos[a], Sam Grimaldo[a], Sandeep Kumar[c,d], Daniel Principe[d], Matthew J. Dorman[a], Ronald McKinney[a], Emilio Hirsch[e], David Dawson[f,g], Hidayatullah G. Munshi[h], Ajay Rana[c,d], and Paul J. Grippo[a,1]

[a]Department of Medicine, Division of Gastroenterology and Hepatology, University of Illinois at Chicago, Chicago, IL 60612; [b]Department of Medicine, Division of Endocrinology, Diabetes and Metabolism, University of Illinois at Chicago, Chicago, IL 60612; [c]Research, Jesse Brown VA Medical Center, Chicago, IL 60612; [d]Department of Surgery, Division of Surgical Oncology, University of Illinois at Chicago, Chicago, IL 60612; [e]Molecular Biotechnology Center, Department of Molecular Biotechnology and Health Sciences, University of Turin, 10126 Turin, Italy; [f]Department of Pathology and Laboratory Medicine, David Geffen School of Medicine, University of California, Los Angeles, CA 90095; [g]Jonsson Comprehensive Cancer Center, David Geffen School of Medicine, University of California, Los Angeles, CA 90095; and [h]Department of Medicine, Northwestern University, Chicago, IL 60611

Edited by Ronald A. DePinho, University of Texas MD Anderson Cancer Center, Houston, TX, and approved May 23, 2019 (received for review August 1, 2018)

Pancreatic ductal adenocarcinoma (PDAC) is notorious for its poor survival and resistance to conventional therapies. PI3K signaling is implicated in both disease initiation and progression, and specific inhibitors of selected PI3K p110 isoforms for managing solid tumors are emerging. We demonstrate that increased activation of PI3K signals cooperates with oncogenic Kras to promote aggressive PDAC in vivo. The p110γ isoform is overexpressed in tumor tissue and promotes carcinogenesis via canonical AKT signaling. Its selective blockade sensitizes tumor cells to gemcitabine in vitro, and genetic ablation of p110γ protects against Kras-induced tumorigenesis. Diet/obesity was identified as a crucial means of p110 subunit up-regulation, and in the setting of a high-fat diet, p110γ ablation failed to protect against tumor development, showing increased activation of pAKT and hepatic damage. These observations suggest that a careful and judicious approach should be considered when targeting p110γ for therapy, particularly in obese patients.

pancreatic cancer | hepatotoxicity | PI3Kg | high-fat diet | AKT signaling

Pancreatic ductal adenocarcinoma (PDAC) has a dismal prognosis, with a median survival of 6 mo (1). This is largely attributed to frequent diagnosis at late stages, as well as widespread resistance to conventional therapy (2) through several emerging mechanisms (3). Recent research has focused on identifying novel molecular targets in the hope of extending patient survival and reducing disease morbidity. Although KRAS mutations are observed in nearly all patients with PDAC, pharmacologic inhibition of KRAS has been elusive, despite some success in animal models (4). As an alternative to KRAS inhibition, proteins that act upstream or downstream of KRAS continue to be investigated as potential candidates for therapy.

Oncogenic KRAS signaling propagates through several effector systems (5, 6). Although multiple arms of RAS signals are required for tumor initiation, activation of the downstream phosphatidylinositol-4,5-bisphosphate 3-kinase (PI3K) pathway appears to be sufficient for tumor maintenance (7). To this end, increased activation of PI3K signals is one of the most frequent occurrences in all human cancers (8). PI3K family members play important roles as regulators of RAS-mediated cell cycle entry and cell growth, survival, and metabolism (9). Once activated, PI3K phosphorylates phosphatidylinositol 4, 5-bisphosphate (PIP2) to generate phosphatidylinositol (3–5)-trisphosphate (PIP3), allowing for the subsequent phosphorylation and activation of Phosphoinositide-Dependent Kinase-1 (PDK1). Active PDK1 then phosphorylates Protein Kinase B (AKT), allowing for the transmission of a variety of downstream signals (10).

There are four mammalian class I PI3K catalytic isoforms (p110s), each found in a heterodimeric complex with a regulatory subunit. While the p110α and β are ubiquitously expressed, p110γ and δ are found predominantly in macrophages and leukocytes, although an increasing number of studies show that p110γ is also expressed to varying degrees in other cell types (11, 12), including pancreatic islets (13, 14), where its biological function is still not fully appreciated. Class IA PI3Ks can be activated downstream of receptor tyrosine kinases (RTKs), G protein-coupled receptors (GPCRs), and small GTPases (15). All catalytic PI3K isoforms contain an RAS-binding domain, although only p110α, δ, and γ isoforms are directly stimulated by RAS (16). This is particularly noteworthy in the context of PDAC, in which approximately 50% of patients harbor overactive PI3K signaling associated with poor outcomes (17, 18) and chemoresistance (19). Traditionally, p110α, β, and δ are linked to RTKs, while p110γ is selectively recruited to GPCRs (20). However, research points to the existence of certain degree of redundancy among the different isoforms. Thus, p110β and p110γ can couple to the same GPCR. As p110β is more broadly distributed, it could provide a conduit for GPCR-linked PI3K signaling in the many cell types where p110γ expression is low or absent (21).

While PI3K signals are most commonly linked to cancer cell proliferation, recent evidence suggests that PI3K also mediates several additional cell functions critical for disease pathogenesis, particularly with respect to immune function (22–24). Several groups have created knockout mouse models of the different class I PI3K subunits describing the phenotypes associated with the loss of each subunit (reviewed in ref. 25). For example, regarding p110γ, mice lacking the PI3Kγ catalytic subunit exhibit

Significance

Although activation of PI3K p110α appears to promote pancreatic cancer development via canonical AKT signaling, in the setting of a high-fat diet (enriched in ω−6 fatty acids), unopposed p110γ inhibition poses a risk for severe hepatic damage. Considering that obesity is a risk factor for pancreatic cancer, these observations suggest the need for caution when translating drugs targeting p110γ to the clinic.

Author contributions: C.T. and P.J.G. designed research; C.T., G.M., J.C.-C., N.V., K.C., S.G., S.K., D.P., M.J.D., and R.M. performed research; C.T., E.H., H.G.M., A.R., and P.J.G. contributed new reagents/analytic tools; C.T. and D.D. analyzed data; and C.T. and P.J.G. wrote the paper.

The authors declare no conflict of interest.

This article is a PNAS Direct Submission.

[1]To whom correspondence may be addressed. Email: ctp@ugr.es or pgrippo@uic.edu.

This article contains supporting information online at www.pnas.org/lookup/suppl/doi:10.1073/pnas.1813012116/-/DCSupplemental.

Published online July 2, 2019.

defects in neutrophil and monocyte migration, along with accumulation in inflamed and tumor tissues (26). In addition, T cells with genetic ablation of p110γ have severely impaired chemotaxis (27), which may alter tumor progression. Studies with these mice have helped unravel the different roles in cellular signaling, growth, and oncogenic transformation of different PI3K isoforms. As inflammation is a key driver of KRAS activation and the PDAC phenotype (28), p110γ inhibition has been proposed as a potential means of reducing pancreatitis as well as cancer-associated inflammation (29), and this approach has shown early efficacy in vivo (30).

The purpose of the present study was to determine the overall effect of p110γ deficiency on the cancer phenotype, as well as to establish any potential adverse effects precipitated by p110γ ablation. To accomplish this, we first assessed the relative expression of p110γ in PDAC databases, followed by a small cohort of PDAC patients, transgenic mouse tumors, and commercially available pancreatic cancer cell lines. We then explored the contributions of the p110γ isoform to epithelial carcinogenesis and chemosensitivity in vitro. When KC mice were crossed to those with either partial or full genetic ablation of p110γ (KC/p110$\gamma^{+/-}$ and KC/p110$\gamma^{-/-}$, respectively), we observed a significant reduction in the neoplastic phenotype with respect to both lesion size and frequency. This was paralleled by reductions in both intratumoral inflammation and activation of the AKT pathway.

The P.J.G. laboratory has previously described the impact of a high-fat diet (HFD) enriched in polyunsaturated fatty acids on the progression of pancreatic neoplasia (31–34). Given the connection between obesity and PI3K, this study includes cohorts of mice on an HFD enriched with ω-6 fatty acids. This diet overwhelmed the protective phenotype observed in pancreases of p110γ-deficient mice. Beyond the lack of a protective effect, these mice also likely had severe defects in both glucose metabolism and lipid metabolism. Taken together, these findings suggest that a cautious approach for p110γ-targeted therapy should be considered, particularly given the potential for reduced efficacy and the likelihood of hepatic/metabolic consequences in obese patients and/or those with nonalcoholic fatty liver disease (NFLD).

Results

Activation of p110α Accelerates Initiation of Pancreatic Neoplasia. PI3K is well accepted as a key driver of the malignant phenotype; however, little work has been done to study this relationship in vivo. To determine whether increased activation of AKT signals is sufficient to accelerate pancreatic intraepithelial neoplasia (PanIN) progression, we crossed *p48-Cre/LSL-KRas^{G12D}* mice (KC mice) to those harboring a constitutively active PI3K p110α subunit (as described in ref. 35) targeted to the pancreatic epithelium (LSL-p110^{CA}) to generate KC/p110^{CA}. At 9 months of age, consistent with previous reports, KC mice developed extensive PanIN1 lesions with the occasional presence of PanIN2 yet retained some normal tissue architecture (40% normal parenchyma compared with B6 animals; $P = 0.001$). In contrast, 100% of KC/p110α^{CA} mice developed more advanced disease, with less percent of residual intact acinar parenchyma (40% in KC mice vs. 20% in KC/p110α^{CA} mice; $P = 0.05$) and with enhanced leukocyte infiltration (Fig. 1 *A* and *B* and *SI Appendix*, Fig. S1 *A–C*). In addition, KC/p110^{CA} had pronounced fibrosis, as shown by COL1A immunostaining and picrosirius red/fast green staining (Fig. 1 *C–E*) both demonstrating a twofold increase ($P = 0.001$). As expected, KC/p110^{CA} mice also displayed enhanced AKT activation, with a significant 1.5-fold increase in pAKT immunostaining (Fig. 1 *C* and *G*; $P = 0.0358$) and a twofold increase on Western blot analysis (Fig. 1 *H* and *I*; $P = 0.05$) as well as increased cell proliferation (PCNA staining, $P = 0.0357$) in neoplastic tissues (Fig. 1 *C* and *F*). However, like

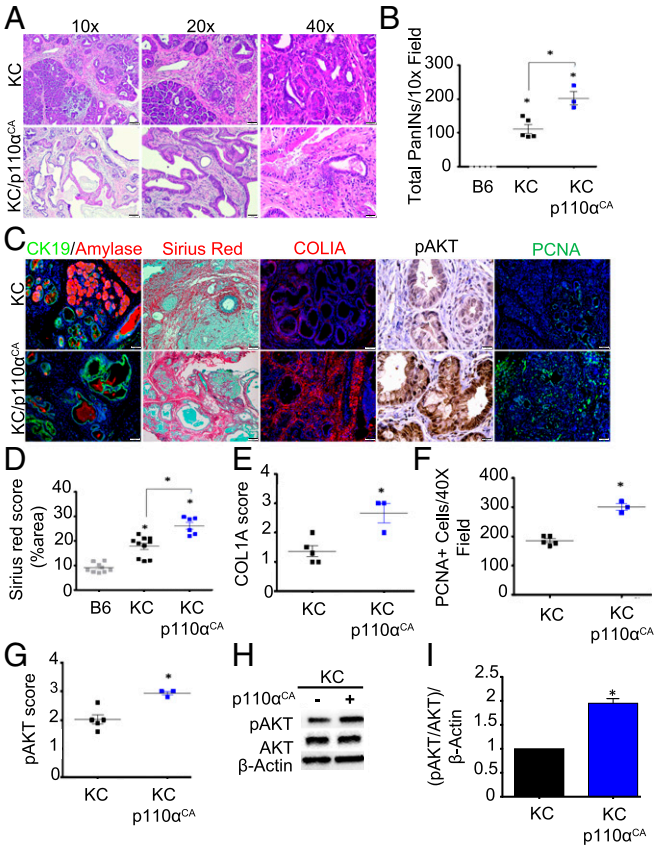

Fig. 1. Constitutive activation of PI3K leads to pancreatic carcinogenesis in vivo. (*A*) Pancreases from KC ($n = 5$) and KC/p110α^{CA} ($n = 3$) mice were evaluated by hematoxylin and eosin (H&E) staining and scored by a pathologist (D.D.) for total number of PanIN (PanIN1-3) lesions. (*B*) The number of neoplastic lesions were counted per high-power field of five different fields of view and averaged. KC vs. B6, $P = 0.001$; KC vs. KC/p110α^{CA}, $P = 0.05$; KC/p110α^{CA} vs. B6, $P < 0.0001$. (*C*) IHC/immunofluorescence for CK19/amylase, picrosirius red/fast green, Col1a, pAKT, and PCNA ($n = 4$). (*D*) Picrosirius red was scored as percent of area. A macro has been applied to quantify the red-stained tissue slides by ImageJ software. This macro segments the red-stained regions using an adjusted threshold after converting images to grayscale (decomposing in RGB components). Finally, the determined red-stained area was calculated and normalized by the entire area of the images. The macro is provided in *SI Appendix*. KC vs. B6, $P < 0.0001$; KC vs. KC/p110α^{CA}, $P = 0.001$; KC/p110α^{CA} vs. B6, $P < 0.0001$. (*E–G*) IHC for Col1a (*E*) and pAKT (*G*) were scored from 0 to 3+ (0, no detectable immunostaining; 1, 10–30% immunostaining; 2, 30–60% immunostaining; 3, >60% immunostaining), and cells were stained for PCNA and evaluated for the number of positive nuclei per high-power field (five different fields of view) (*F*). KC vs. KC/p110α^{CA}, $P = 0.001$ (*E*); KC vs. KC/p110α^{CA}, $P = 0.0357$ (*F*); KC vs. KC/p110α^{CA}, $P = 0.0358$ (*G*). (*H*) Pancreas lysates from KC ($n = 4$) and KC/p110α^{CA} ($n = 3$) mice were isolated, and pAKT expression was analyzed by immunoblotting. (*I*) Quantification of the replicates performed by immunoblotting relative to GAPDH expression level. Quantification was done with ImageJ software. All images are representative of the averaged results of the scoring of KC ($n = 5$) and KC/p110α^{CA} ($n = 3$) mice. KC vs. KC/p110α^{CA}, $P = 0.05$. In this and all other figures, asterisks in the graphs above a group define significance against the first group, used as control. All other significant differences are defined with bars across the top of the appropriate groups.

KC mice, KC/p110α^{CA} mice displayed only an occasional presence of PanIN2, with no detectable microscopic PDA foci.

PI3K p110γ Is Up-Regulated in Pancreatic Cancer Patients. As individual PI3K subunits are being proposed as potential targets for therapy, we first evaluated expression of various PI3K isoforms using well-established patient databases that were confirmed

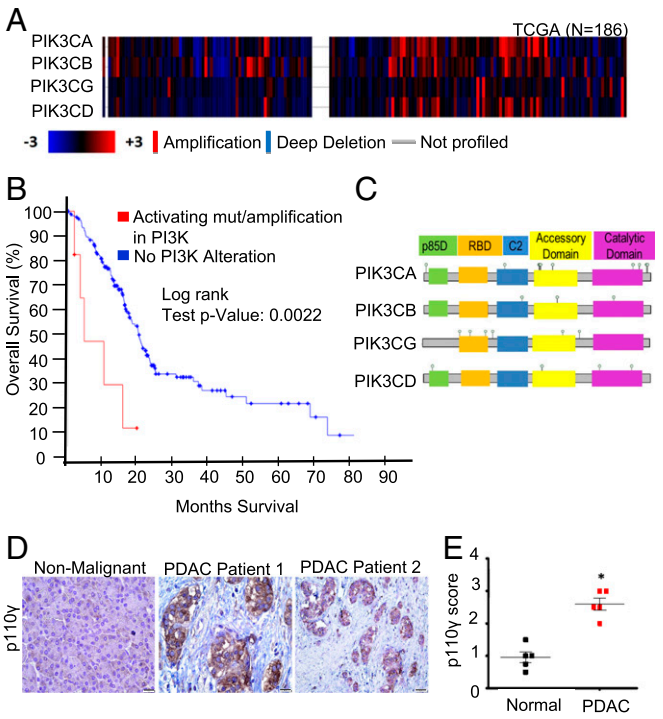

Fig. 2. PI3K p110γ is up-regulated in patients with PDAC. (*A*) Copy number alteration (CNA) among four PI3K gene isoforms—p110α (PIK3CA), p110β (PIK3CB), p110γ (PIK3CG), and p110δ (PIK3CD)—in 186 patients with PDAC represented as a heatmap, which was obtained from the provisional TCGA database from cBioPortal (http://www.cbioportal.org). The CNA analysis was performed using putative CNAs from GISTIC2 (Genomic Identification of Significant Targets in Cancer) that assign the following values: −2 = homozygous deletion; −1 = hemizygous deletion; 0 = neutral /no change; 1 = gain; 2 = high level amplification. The heatmap displays log2 copy numbers. (*B*) Kaplan–Meier survival curve generated by the cBioPortal. Shown are the overall fractions of subjects surviving over time with and without alterations in the four PI3K gene isoforms: PIK3CA, PIK3CB, PIK3CG, and PIK3CD. The alterations include amplifications and activating mutations. A robust difference in survival across groups was observed in the patients with PDAC ($P = 0.0022$). (*C*) Identified p110 alterations and their locations in the combined dataset. p85-BD, p85-binding regulatory domain; RBD, RAS-binding domain. (*D* and *E*) IHC evaluation of p110γ expression in adjacent nonmalignant and PDAC tumor tissue scored from 0 to 3+ (0, no detectable immunostaining; 1, 10–30% immunostaining; 2, 30–60% immunostaining; 3, >60% immunostaining). $n = 5$/group; PDAC vs. normal, $P = 0.0119$.

using primary PDAC patient samples. By mining the TCGA dataset ($n = 185$), we found that copy number alteration of the four PI3K p110 isoforms is common, but not uniformly present in all PDAC patients (Fig. 2*A*). We then combined these results with the UTSW, QCMG, and ICGC datasets and evaluated the combined set of 850 patients for genomic alterations to the p110 subunits. We found that up to 25% of patients harbor genomic alterations to one or more p110 isoforms (*SI Appendix*, Fig. S2*A*). Of these alterations, copy number amplification was the most common, particularly with respect to p110α (PIK3CA) and p110γ (PIK3CG) (*SI Appendix*, Fig. S2*A*). Patients with amplifications/activating mutations in PI3K had reduced overall survival (4.7 vs. 20.17 mo) compared with those without p110 alterations (Fig. 2*B*). We identified a total of 31 p110 mutations across the combined patient cohort (Fig. 2*C* and *SI Appendix*, Fig. S2*B*).

Missense mutations occur in all domains of p110α, but the majority cluster in two hotspots, with the most common E542K and E545K in the helical domain and H1047R in the kinase domain (36). These hotspot mutations confer transformation via constitutive activation of p110α (37, 38). Helical domain mutations reduce the inhibition of p110α by p85 or facilitate the direct interaction of p110α with insulin receptor substrate 1, while kinase domain mutations increase the interaction of p110α with lipid membranes. Other PIK3CA mutations mimic distinct structural conformation changes occurring during activation of PI3K. For p110γ (PIK3CG), most mutations are clustered near the RAS-binding domain (Fig. 2*C*), but the specific consequences of these mutations require further research. Of these 31 mutations, seven occur in amino acids that have previously been associated with oncogenic function in other cancers, although the remaining mutations are uncharacterized and their biologic consequences unknown (Fig. 2*C* and *SI Appendix*, Fig. S2*B*).

While p110α and p110β are ubiquitously expressed and known to drive PDAC development, the alterations to p110γ were unexpected, as this isoform is often associated with macrophages and leukocytes, not with the cancer epithelium. Therefore, we assessed the expression of p110γ in both PDAC ($n = 5$) and adjacent normal tissues ($n = 5$) by immunohistochemistry (IHC). Slides were scored based on intensity from 0 (nonexpressing) to 3+ (strong expression), and scores were averaged. Consistent with the genomic data, the mean expression of p110γ was significantly elevated in PDAC sections compared with adjacent normal tissue ($P = 0.0119$), with staining for p110γ localized strongly to the cancer epithelium as well as the inflammatory infiltrate (Fig. 2 *D* and *E*).

Epithelial p110γ Promotes AKT Activation In Vitro. As most of our patient cohort expressed p110γ in the cancer epithelium, we next assessed the basal expression of the three most clinically relevant p110 isoforms in Panc-1, MiaPaca-2, and AsPC-1 PDAC cell lines by immunocytochemistry, Western blot analysis (Fig. 3 *A* and *B* and *SI Appendix*, Fig. S3*B*), and RT-PCR (*SI Appendix*, Fig. S3*A* and Table S2). Although each p110 isoform was expressed in all cell lines, the patterns of expression varied. In general, according to protein levels assessed by Western blot analysis (Fig. 3*B* and *SI Appendix*, Fig. S3*B*), these 3 cell lines expressed p110β at higher levels. Panc-1 showed low levels of p110α, similar to those in MiaPaca-2, and with higher levels in AsPC-1. In contrast,

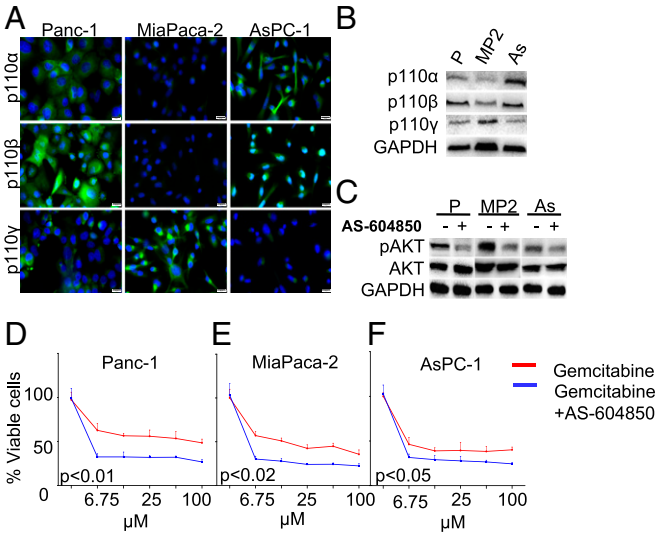

Fig. 3. Epithelial p110γ promotes AKT activation in vitro. (*A* and *B*) Expression of p110α, p110β, and p110γ in Panc-1 (P), MiaPaca-2 (MP2), and ASPC-1 (As) cancer cell lines was evaluated by immunofluorescence (*A*) and Western blot (*B*) analyses. (*C*) Cancer cell lines were administered 0.25 μM of the selective p110γ inhibitor AS-604850, and downstream pathway inhibition (pAKT level) was determined by Western blot analysis. (*D*–*F*) Cancer cell lines were preincubated for 1 h with 0.25 μM AS-604850 supplemented with increasing doses of gemcitabine, and cell viability was determined by an MTT assay. All assays were performed in triplicate, and the results were averaged.

Panc-1 cells expressed p110β at higher levels than p110α and p110γ. MiaPaca-2 had high protein levels of p110γ with lower levels of p110α and p110β. AsPC-1 had higher levels of p110α and p110β and lower levels of p110γ with similarly high levels in MiaPaca-2 and AsPC-1. p110γ was expressed at low levels in AsPC-1 cells, at intermediate levels in Panc-1 cells, and at high levels in MiaPaca-2 cells (Fig. 3 *A* and *B* and *SI Appendix*, Fig. S3 *A* and *B*).

To determine the biological importance of p110γ in these different cell lines, we first administered the selective ATP-competitive PI3Kγ inhibitor AS-604850 and evaluated the effects on downstream AKT signaling. Although AS-604850 does not solely inhibit p110γ, it has >30-fold selectivity over PI3Kδ and PI3Kβ and 18-fold selectivity over PI3Kα (39). As a single agent and at 0.25 μM (the concentration at which AS-604850 specifically inhibits only the p110γ isoform), the drug did not affect viability (*SI Appendix*, Fig. S3*C*). Despite the varied p110γ expression among the cell lines, AS-604850 significantly halved AKT phosphorylation in all cell lines (Fig. 3*C* and *SI Appendix*, Fig. S3*D*). Similarly, AS-604850 sensitized Panc-1 and MiaPaca-2 cell lines to treatment with gemcitabine (50 μM), although there was a reduced effect on the p110γ-low AsPC-1 cell line (Fig. 3 *D*–*F*).

Genetic Ablation of p110γ Reduces PanIN Formation and Disrupts AKT Pathway Activation In Vivo. p110γ appears sufficient to promote AKT pathway activation in vitro. To determine whether p110γ is required for AKT signaling in vivo, we first assessed basal expression of p110γ in the pancreas of wild-type (WT) control, p48-Cre/LSL-KRAS^{G12D} (KC), and p48-Cre/LSL-KRAS^{G12D}/LSL-TP53^{R172H} (KPC) mice at age 4 mo. In both disease models, p110γ expression was significantly up-regulated (KC and KPC vs. B6, P = 0.0486 and 0.0112, respectively; KC vs. KPC, P = 0.0339), again localized to epithelial and inflammatory cells, as assessed by IHC (Fig. 4 *A* and *B*) and Western blot analysis (*SI Appendix*, Fig. S4 *A* and *B*). Therefore, we crossed KC mice to mice harboring either deletion of the p110γ isoform to generate

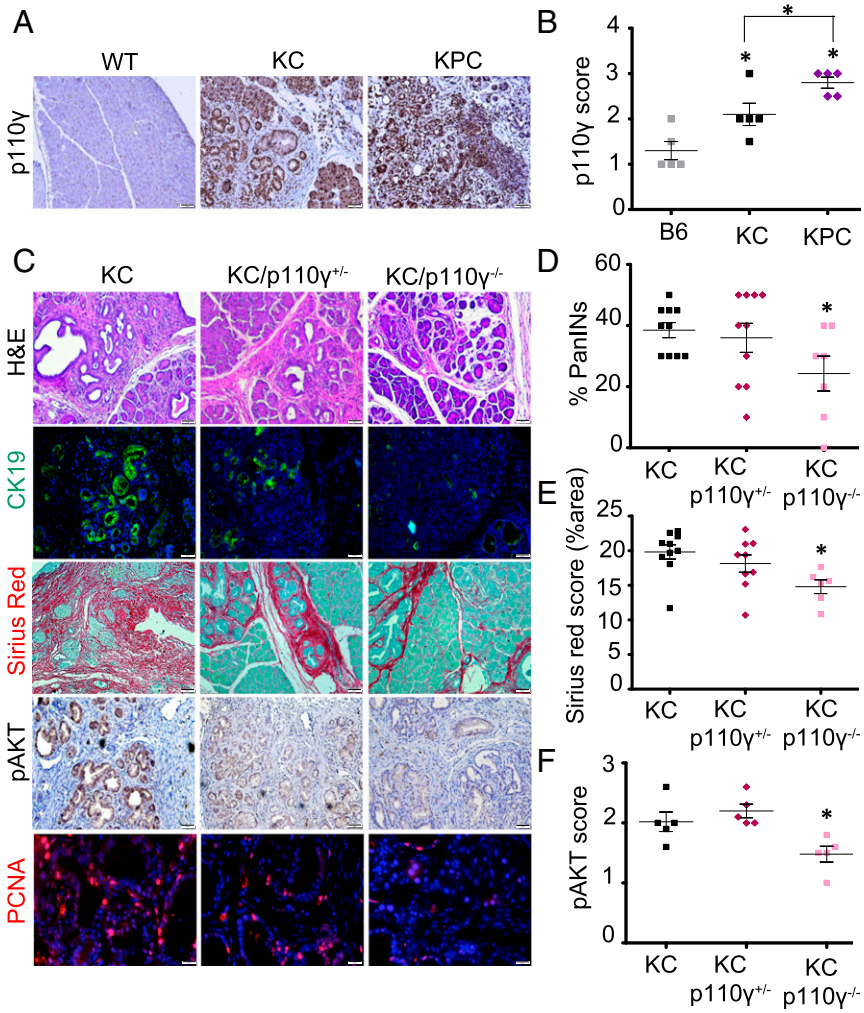

Fig. 4. Genetic ablation of p110γ reduces PanIN formation and disrupts AKT pathway activation in vivo. (*A* and *B*) Pancreas sections from 4-mo-old nongenic control (B6; n = 5), p48-Cre/LSL-KRAS^{G12D} (KC; n = 5), or p48-Cre/LSL-KRAS^{G12D}/LSL-TP53^{R172H} (KPC, n = 5) mice were stained for p110γ (*A*) and scored from 0 to 3+ (*B*) (0, no detectable immunostaining; 1, 10–30% immunostaining; 2, 30–60% immunostaining; 3, >60% immunostaining). The numerical scoring represents the average of two independent investigators (C.T. and D.P.), and five different fields of view. KC and KPC vs. B6, P = 0.0486 and P = 0.0112, respectively; KC vs. KPC, P = 0.0339. (*C*) KC, KC/p110γ$^{+/-}$, and KC/p110γ$^{-/-}$ pancreases (n = 10, 10, and 7, respectively) were similarly stained with H&E, with the ductal marker CK19 (n = 5 of each), picrosirius red/fast green, pAKT, and for proliferation via PCNA (n = 5). (*D*) The number of neoplastic lesions was scored by a pathologist (D.D.) for total number of PanIN (PanIN1–3) lesions. KC/p110γ$^{-/-}$ vs. KC, I = 0.0201. (*E*) Picrosirius was scored and quantitated using a modification of the macro provided in *SI Appendix* (https://imagej.nih.gov/ij/docs/examples/stained-sections/index.html) to automatically score the fibrosis index as percentage of area. KC/p110γ$^{-/-}$ vs. KC, P = 0.0047. (*F*) pAKT was scored from 0 to 3+ (P = 0.0273, KC vs. KC/p110γ$^{-/-}$), similar to p110γ. KC/p110γ$^{-/-}$ vs. KC, P = 0.0273. All of the images were taken at 20× and are representative of the results of the averaged score.

KC/p110γ$^{+/-}$ and KC/p110γ$^{-/-}$, respectively, and assessed the effects on early tumorigenesis as well as on downstream activation of the AKT pathway. Consistent with previous reports (30), KC/p110γ$^{-/-}$ mice had significant reductions in lesion frequency (less PanIN1, $P = 0.0054$; fewer total PanINs lesions, $P = 0.0201$; Fig. 4 *C* and *D*), inflammation, and fibrosis ($P = 0.0047$; Fig. 4 *C* and *E*) compared with age-matched KC controls, with KC/p110γ$^{+/-}$ mice displaying an intermediate phenotype, although the differences did not achieve significance ($P = 0.6941$; Fig. 4 *C* and *D*). This was paralleled in the EL-KRAS^{G12D} (EK) model of cystic papillary neoplasia, in which p110γ deficiency also protected against tumor formation (*SI Appendix*, Fig. S4*E*). KC mice had strong expression of the downstream p110γ target pAKT (Fig. 4 *C* and *F*), concomitant with increased cell proliferation (via PCNA staining; *SI Appendix*, Fig. S4*D*) in neoplastic tissues. Both proteins were significantly reduced in KC/p110γ$^{-/-}$ mice (pAKT KC vs. KC/p110γ$^{-/-}$, $P = 0.0273$; PCNA KC vs. KC/p110γ$^{-/-}$, $P = 0.0079$; Fig. 4 *C* and *F* and *SI Appendix*, Fig. S4*D*), with PCNA also showing significance with KC/p110γ$^{+/-}$ mice (KC vs. KC/p110γ$^{-/-}$, $P = 0.0079$; *SI Appendix*, Fig. S4*D*). These results were recapitulated by Western blot analysis (Fig. 5 *A* and *B*).

p110γ Deficiency Fails to Protect against Pancreatic Carcinogenesis in the Setting of HFD. Since HFDs have been associated with increased AKT activation, we sought to determine whether the observed protective effect via p110γ loss would persist in the same cohort of mice administered an HFD. To determine whether p110γ specifically was required for the aggressive phenotype, KC (Fig. 5*C*, *Left*), KC/p110γ$^{+/-}$(Fig. 5*C*, *Center*), and

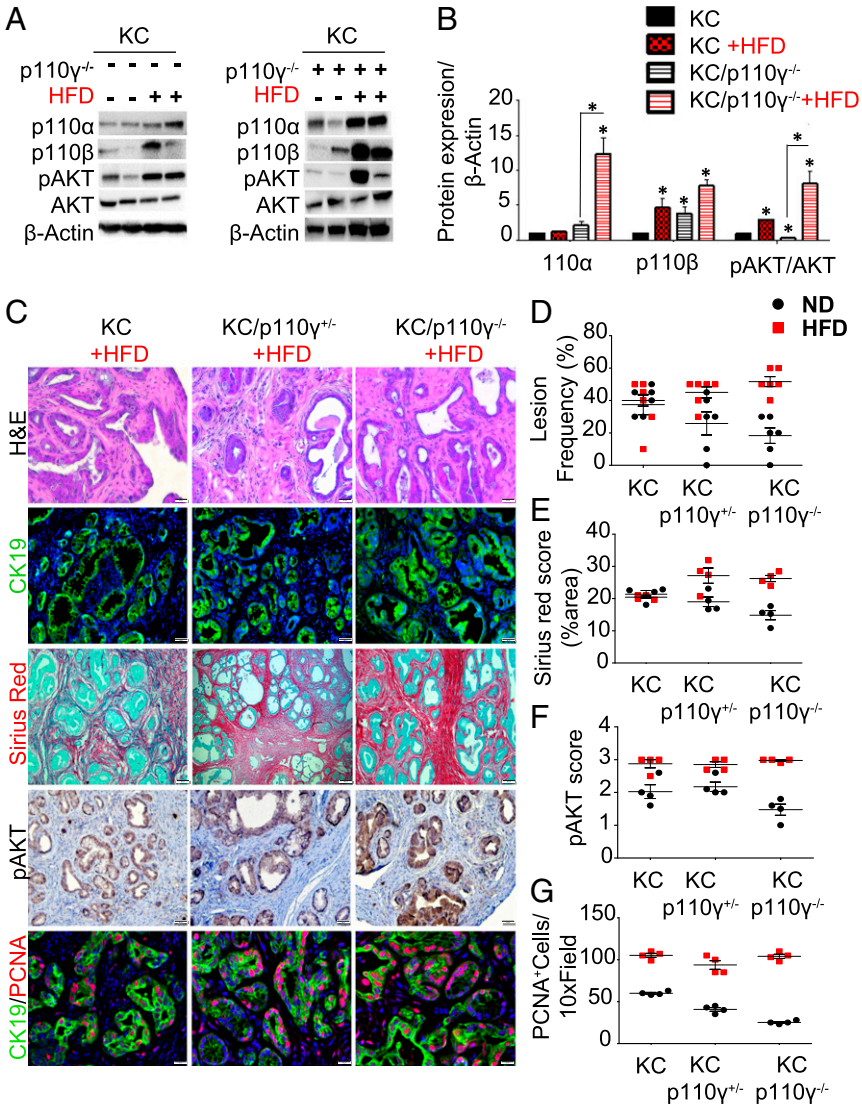

Fig. 5. p110γ deficiency fails to protect against pancreatic carcinogenesis in the setting of an HFD. p48-Cre/LSL-KRAS^{G12D} (KC), KC/p110γ$^{+/-}$, and KC/p110γ$^{-/-}$ mice were fed an HFD (red squares). (*A*) Pancreas protein lysates were obtained from KC and KC/p110 γ$^{-/-}$ mice on either an ND or an HFD ($n = 4$) (duplicates shown) and levels of p110α, p110β, AKT, and pAKT were also assessed by immunoblotting. (*B*) Western blot quantification relative to β-actin. Quantification was done with ImageJ. This represents the measurement of three independent replicates. All comparisons are made against KC ND, and the significance reflects this comparison. (*C*) Pancreases were evaluated histologically by H&E ($n = 6$) or stained for CK19, picrosirius red/fast green, pAKT, or PCNA ($n = 4$). (*D*–*F*) Sections were quantified and compared with mice on the control diet (black dots) for lesion frequency (*D*), fibrosis by sirius red/fast green staining scored according to the automatic macro implemented (*E*), and phosphorylated AKT, scored from 0 to 3+ (0, none detected; 1, 10–30%; 2, 30–60%; 3, >60%) (*F*). The numerical score represents the average of two independent investigators (C.T. and D.P.). (*G*) PCNA evaluated for the number of positive nuclei per high-power field (five different fields of view). *$P < 0.05$.

KC/p110γ$^{-/-}$ (Fig. 5*C*, *Right*) mice were administered the HFD for 8 mo, and both KC/p110γ$^{+/-}$ and KC/p110γ$^{-/-}$ developed highly advanced disease forms histologically indistinct from KC+HFD age-matched controls [Fig. 5*D*; normal diet (ND), black spots; HFD, red squares]. In each case, mice exhibited near-complete loss of normal gland parenchyma, with only marginal reductions in lymphocyte infiltration (*SI Appendix*, Fig. S5*A*). In addition, these mice displayed robust AKT activation in the pancreas, which was significant when compared against age- and genotype-matched groups as shown by immunostaining (KC/p110γ$^{-/-}$ ND vs. KC/p110$^{-/-}$ HFD, $P = 0.0286$) and Western blots (Fig. 5 *A*–*C* and *F*), further indicating that the HFD is driving AKT pathway activation through alternate p110 isoforms. Consistent with these findings, there was no significant difference in cell proliferation in any group administered the HFD (Fig. 5 *C* and *G*). Similar results were observed in EK, EK/p110γ$^{+/-}$, and EK/p110γ$^{-/-}$ mice, which also developed more advanced disease forms in response to the HFD (*SI Appendix*, Fig. S5*B*). To determine what isoform could be mediating pAKT recovery, we assessed protein expression of p110α and p110β in the pancreases of KC and KC/p110γ$^{-/-}$ mice. Our results show increased levels of p110β regardless of p110γ, most likely due to the HFD (KC vs. KC HFD, vs. KC/p110γ$^{-/-}$, and vs. KC/p110γ$^{-/-}$ HFD, all significant, with $P = 0.0286$ for all comparisons). However, KC/p110γ$^{-/-}$ vs. KC/p110γ$^{-/-}$ HFD did not achieve significance, $P = 0.0571$; Fig. 5 *A* and *B*). On the other hand, p110α was specifically induced in KC/p110$^{-/-}$ HFD, with a 12-fold increase (Fig. 5 *A* and *B*) showing a significant change when comparing KC/p110γ$^{-/-}$ vs. KC/p110γ$^{-/-}$ HFD ($P = 0.0286$) but not achieving significance when compared with the other groups ($P > 0.05$).

p110γ Inhibition in the Setting of an HFD Leads to Hyperactivation of AKT from Compensation through Alternate p110 Isoforms. As the HFD appears to establish a tumor permissive phenotype and activate AKT signaling independent of p110γ, we next evaluated the effects of in vitro p110γ inhibition when combined with administration of the main component of the in vivo HFD: ω-6 polyunsaturated fatty acids, in this case, linoleic acid (LA). We again used Panc-1, MiaPaca-2, and AsPC-1 PDAC cell lines and administered 40 μM of LA, the working concentration as previously determined empirically in our laboratory (34). In response to LA, each cell line displayed increased expression of p110α, p110β, and p110γ both at the mRNA (Fig. 6 *A*–*C*) and protein levels (Fig. 6*D* and *SI Appendix*, Fig. S6 *A*–*D*). These changes were associated with increased AKT activation in response to LA (Fig. 6*D* and *SI Appendix*, Fig. S6 *B*–*D*). Although p110γ inhibition lowered pAKT expression in these three cell lines when administered as a single agent, when combined with LA, p110γ inhibition led to increased LA-induced up-regulation of p110α and p110β and failed to prevent LA-induced AKT phosphorylation (Fig. 6*D* and *SI Appendix*, Fig. S6 *B*–*D*). Consistent with our animal data, analysis of the cell lines showed that p110β expression in vitro was induced after LA treatment compared with after BSA and after LA+AS-604850, and there was no significant change between the latter (for Panc-1, $P = 0.2000$, *SI Appendix*, Fig. S6*B*; for MiaPaca-2, $P = 0.8$, *SI Appendix*, Fig. S6*C*; for AsPC-1, $P = 0.4857$, *SI Appendix*, Fig. S6*D*). However, p110α was significantly induced after LA treatment compared with BSA, but the combination of LA with the p110γ inhibitor also showed significantly higher levels of protein compared with LA alone (for Panc-1, $P = 0.0286$, *SI Appendix*, Fig. S6*B*; for MiaPaca-2, $P = 0.0286$, *SI Appendix*, Fig. S6*C*; for AsPC-1, $P = 0.037$, *SI Appendix*, Fig. S6*D*). Taken together, these findings suggest that there may be little benefit to p110γ inhibition in the setting of an HFD and/or obesity, likely due to compensation through alternate p110 isoforms.

To investigate whether other p110 isoforms were responsible for the recovery of AKT phosphorylation, Panc-1 and MiaPaca-2

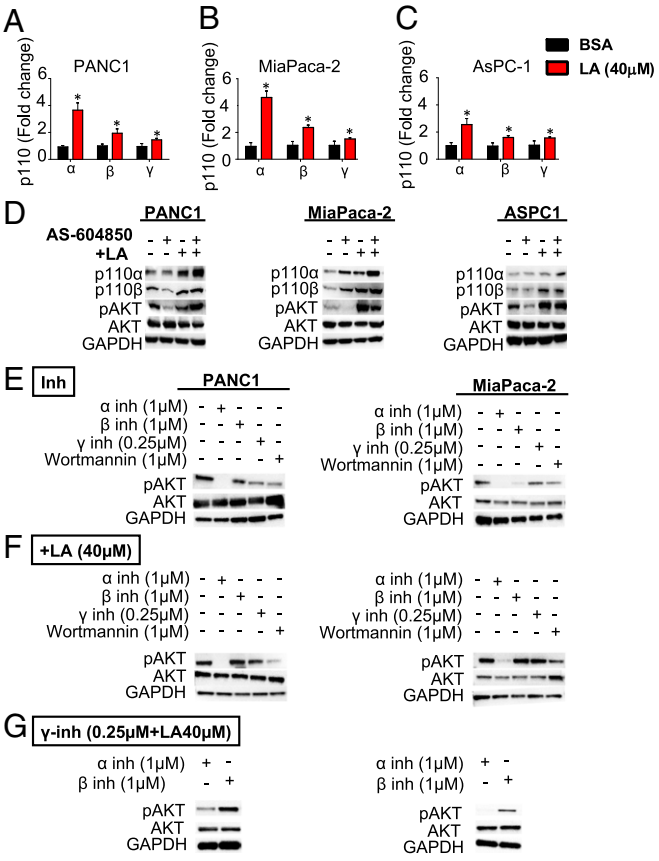

Fig. 6. Exogenous supplementation of ω-6 fatty acids activates the AKT pathway. (*A*–*C*) Panc-1 (*A*), MiaPaca-2 (*B*), and AsPC-1 (*C*) cells were treated with LA (40 μM), and p110α, p110β, and p110γ expression in vitro was evaluated by qPCR. (*D*) Panc-1, MiaPaca-2, and AsPC-1 cells were treated with LA 40 μM, the p110γ specific inhibitor AS-604850 (0.25 μM), or a combination of the two, and P110α and p110β expression in vitro was evaluated by Western blot analysis, which also shows AKT activation as determined by pAKT levels. (*E*) pAKT is activated by an alternate p110 isoform after γ-inhibition in the setting of HFD. Panc-1 and MiaPaca-2 were incubated with p110-isoform specific inhibitor p110α (BYL719) or p110β (GSK2636771) for 48 h, and pAKT level was assessed by Western blot analysis. (*F*) Panc-1 and MiaPaca-2 were then incubated in the presence of LA (40 μM) for 48 h, and pAKT levels were assessed by Western blot analysis. (*G*) Panc-1 and MiaPaca-2 were then incubated in the presence of AS-604850+LA and either BYL719 or GSK2636771. Increased pAKT was abolished in the presence of BYL719. All assays were performed in triplicate, and the results were averaged. *$P < 0.05$.

cells were treated with different combinations of p110α (BYL719) and p110β (GSK2636771) isoform-selective inhibitors at doses previously shown to selectively discriminate among different isoforms (40, 41) and with a pan-PI3K inhibitor (wortmannin). pAKT levels were suppressed after incubation with the different isoform-specific inhibitors. p110α inhibition was the more potent, suggesting a principal role for p110α in driving pAKT activation in PDAC cells (Fig. 6*E* and *SI Appendix*, Fig. S6 *E* and *F*), as was also seen in the KC/p110α^{CA} mice (Fig. 1). When combined with LA (40 μM), pAKT levels were partially restored after a 48-h treatment with GSK2636771/AS-604850 and the fatty acid, despite the continued presence of the inhibitors. However, when combined with BYL719 or wortmannin, LA was unable to induce a significant increase in pAKT (Fig. 6*F* and *SI Appendix*, Fig. S6 *E* and *F*).

Finally, we assessed pAKT expression in PDAC cells treated with AS-604850 + LA and either BYL719 or GSK2636771. In the presence of the p110β-specific inhibitor, enhanced pAKT

was maintained, while the presence of the p110α-specific inhibitor effectively mitigated high levels of pAKT after 48 h. This suggests that p110α is responsible for AKT phosphorylation in PDAC cells treated with p110γ-specific inhibitor in the presence of LA (Fig. 6*G* and *SI Appendix*, Fig. S6 *E* and *F*).

Loss of p110γ Leads to Diet-Induced Hepatocyte Injury in Tumor-Bearing Mice. Since the liver is typically the first organ with metastasis in patients with PDAC and plays a pivotal role in lipid metabolism, we assessed the hepatic effects of the HFD in our mice cohorts. It has been previously reported that loss of p110γ prevents the onset of insulin resistance, metabolic inflammation, and fatty liver (12). Our report supports these observations in non–tumor-bearing mice fed a standard diet, because weight and plasma levels of insulin, cholesterol, and nonesterified fatty acids (NEFAs), as well as hepatic steatosis and fibrosis were not altered independent of p110γ expression (*SI Appendix*, Fig. S7 *A–F*, black dots, *SI Appendix*, Fig. S7 *G–I*). However, nontumor B6 ($p110\gamma^{+/+}$) mice fed an HFD (red squares) showed increased body weight ($P = 0.0006$, *SI Appendix*, Fig. S7*A*), plasma insulin ($P = 0.0174$, *SI Appendix*, Fig. S7*B*) and cholesterol ($P = 0.008$, *SI Appendix*, Fig. S7*C*) levels than age-matched animals fed a normal diet (ND), with a mean steatosis score of 2 ($P = 0.0117$, *SI Appendix*, Fig. S7 *E* and *H*). Serum levels of NEFAs and fibrosis scored by sirius red staining showed no statistically significant difference (*SI Appendix*, Fig. S7 *D*, *F*, and *G*). Both HFD-fed nontumor $p110\gamma^{+/-}$ and $p110\gamma^{-/-}$ mice showed increased body weight compared with ND-fed genotype-matched mice; however, their body weight was significantly reduced compared with HFD-fed B6 mice ($P = 0.0023$ and 0.0024, respectively; *SI Appendix*, Fig. S7*A*, red squares). Likewise, HFD-fed non–tumor-bearing $p110\gamma^{+/-}$ and $p110\gamma^{-/-}$ mice showed reduced plasma insulin ($P = 0.0043$ and 0.0159, respectively) and cholesterol ($P = 0.0087$ and $P = 0.0079$ respectively) compared with HFD-fed B6 mice (*SI Appendix*, Fig. S7 *B* and *C*, red squares). Serum levels of NEFAs were similarly independent of p110γ expression (*SI Appendix*, Fig. S7*D*, red squares). Finally, there was no sign of steatosis or fibrosis in the livers of non–tumor-bearing animals with p110γ loss on an HFD, corroborating the protective effect in obesity-related symptoms (*SI Appendix*, Fig. S7 *F* and *G*).

Unexpectedly, partial or complete loss of p110γ in the presence of pancreatic neoplasia (KC model) promoted dramatic changes in liver architecture consistent with widespread hepatocyte damage, lipid vacuole accumulation, and steatosis when mice were fed an HFD (Fig. 7 *A* and *B*). Oil red O-stained slides confirmed the development of NAFLD in $KC/p110\gamma^{+/-}$ and $KC/p110\gamma^{-/-}$ mice fed an HFD (Fig. 7*A*). While KC animals on an HFD presented with an average steatosis score of 1.2 (statistically significant compared with KC on an ND; $P = 0.0117$), $KC/p110\gamma^{+/-}$ and $KC/p110\gamma^{-/-}$ mice on an HFD presented with average scores of 2.5 and 2.7, which represent 2-fold and 2.14-fold higher presence of lipid accumulation in the liver, respectively ($P = 0.0196$ and 0.0334, respectively; Fig. 7*B*). In addition, compared with their respective controls, HFD-fed $KC/p110\gamma^{-/-}$ mice showed increased serum cholesterol levels (Fig. 7*C*). $KC/p110\gamma^{-/-}$ mice on an HFD had 2.6-fold higher serum cholesterol levels than aged-matched animals fed an ND ($P = 0.0043$) and 1.8-fold higher levels than KC animals on an HFD ($P = 0.0411$). NEFA serum levels were significantly elevated in $KC/p110\gamma^{+/-}$ and $KC/p110\gamma^{-/-}$ mice on an HFD compared with KC mice on an ND (1.35 and 1.22 mEq/L vs. 0.90 mEq/L; $P = 0.026$ and 0.021, respectively) but did not show significance compared with KC mice on an HFD (Fig. 7*D*). Of note, body weight (*SI Appendix*, Fig. S7*K*) and serum levels of insulin (Fig. 7*E*) did not show significant differences among neoplastic groups regardless of the diet, possibly due to a reduction of pancreatic islets in KC mice. Finally, loss of p110γ expression increased hepatic fibrosis

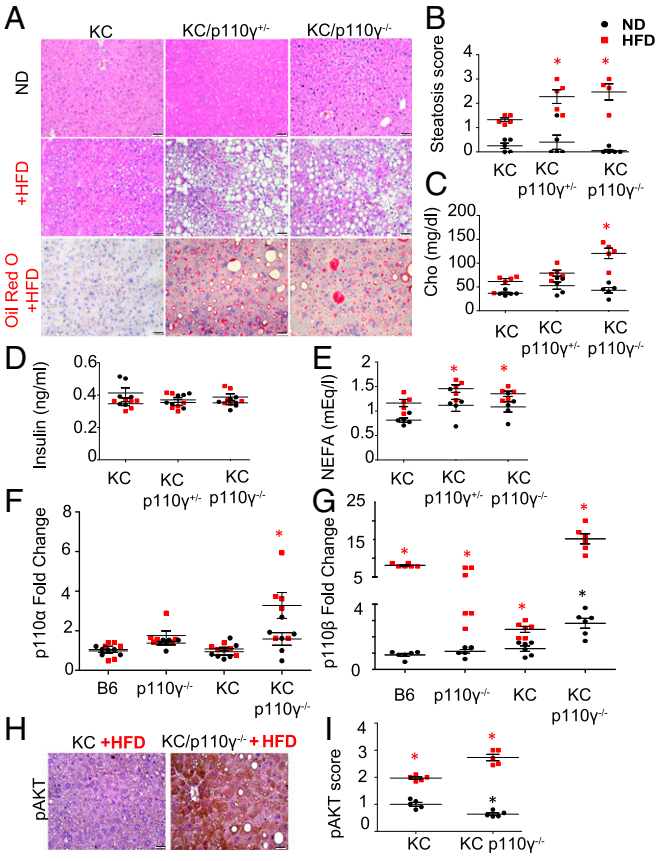

Fig. 7. Loss of p110γ leads to severe diet-induced hepatic injury and lipid accumulation in tumor-bearing mice. (*A* and *B*) Livers from p48-Cre/LSL-$KRAS^{G12D}$ (KC; $n = 4$), $KC/p110\gamma^{+/-}$ ($n = 4$), and $KC/p110\gamma^{-/-}$ ($n = 4$) mice on either the control (ND) or an HFD were stained with H&E (*A*), and frozen liver sections were stained with oil red O and scored from 0 to 3+ for steatosis ($n = 5$) (*B*). This score was on a scale of 0–3 (0, <10%; 1, 10–35%; 2, >35–65%; 3, >65%) based on the degree of vacuolization in the cytoplasm and the degree of distribution of the vacuolated hepatocytes. (*C*) Serum levels of cholesterol in KC, $KC/p110\gamma^{+/-}$, and $KC/p110\gamma^{-/-}$ mice on each diet were evaluated by GC-MS ($n = 5$). (*D*) Serum levels of NEFAs in KC, $KC/p110\gamma^{+/-}$, and $KC/p110\gamma^{-/-}$ mice on each diet were evaluated by GC-MS ($n = 5$). (*E*) Serum levels of Insulin in KC, $KC/p110\gamma^{+/-}$, and $KC/p110\gamma^{-/-}$ mice on each diet was measured by enzyme-linked immunosorbent assay ($n = 6$). (*F* and *G*) Relative liver expression of p110α and p110β in the livers of B6, $p110\gamma^{-/-}$, KC, and $KC/p110\gamma^{-/-}$ mice fed on an HFD was evaluated by qPCR. $n = 5$; $^*P < 0.05$. (*H* and *I*) The livers of KC and $KC/p110\gamma^{-/-}$ mice fed on an HFD were similarly stained via IHC for pAKT (*H*), and the slides were scored from 0 to 3+ (*I*) (0, no detectable immunostaining; 1, 10–30% immunostaining; 2, 30–60% immunostaining; 3, >60% immunostaining). The numerical score represents the average of two independent investigators (C.T. and D.P.). $n = 5$; $^*P < 0.05$. Asterisks in red define significance comparing HFD groups. Asterisks in black define significance comparing ND groups. See *Loss of P110g Leads to Diet-Induced Hepatocyte Injury in Tumor-Bearing Mice* for more detailed comparisons.

in KC mice fed an HFD as determined by sirius red/fastgreen staining (*SI Appendix*, Fig. S7 *I* and *J*). This NAFLD phenotype also was observed in $EK/p110\gamma^{+/-}$ and $EK/p110\gamma^{-/-}$ mice on an HFD (*SI Appendix*, Fig. S8*A*).

Because PI3K/AKT signaling plays a central role in lipid metabolism and has increased activation during pancreatic carcinogenesis, we assessed the relative mRNA expression of the various p110 isoforms. In non–tumor-bearing animals, loss of p110γ in the liver did not affect the expression of any of the other isoforms (Fig. 7 *F* and *G*, black dots). The HFD did not induce any significant change in p110α (Fig. 7*F*) regardless of the genotype; however, it did

induce the expression of p110β as observed in an 8-fold and 4.7-fold increase in B6 and p110γ$^{-/-}$ mice, respectively, compared with B6 and p110γ$^{-/-}$ mice fed an ND (Fig. 7*G*, red dots vs. black squares). In the presence of a Kras mutation, p110α was significantly elevated ($P = 0.0043$) only in KC/p110γ$^{-/-}$ mice on an HFD (Fig. 7*F*, red squares). p110β was up-regulated in KC/p110γ$^{-/-}$ mice on an ND (Fig. 7*G*, black dots), and in the presence of an HFD, there was a 15-fold up-regulation of p110β (Fig. 7*G*, red squares). This was paralleled by increased activation of AKT in intact hepatocytes, which were generally closest to the portal vein (Fig. 7 *H* and *I*). These results point to increased hepatic PI3K/AKT pathway activation in the setting of p110γ loss and HFD, which is likely accompanied by altered lipid and glucose metabolism (*SI Appendix*, Figs. S8 and S9).

Discussion

The p110γ isoform is emerging as a critical but less well-studied mediator of PDAC development. Previous studies have identified central roles for p110γ in regulating various aspects of tumor progression, particularly with respect to its proinflammatory function in macrophages (30). Consistent with our observations, it recently has been demonstrated that human PDAC often displays pronounced overexpression of the p110α and p110γ isoforms (42). While the contributions of p110α to pathogenesis are well-characterized, the role of p110γ beyond the inflammasome is only recently becoming clear. p110γ expression has been observed in patients with inflammation of the pancreas and because of that, it has been proposed that p110γ expression and activation could be an early event that links chronic pancreatitis and pancreatic adenocarcinoma (43). Given the tumor-promoting role of p110γ in PDAC, its inhibition has been proposed as a potential therapy for PDAC and has shown early promise in vivo (30). The potential role of p110γ in both inflammation and tumor development provides an appealing opportunity to target both tumor cell as well as inflammation.

In this work, we found that the p110γ isoform is up-regulated in human PDAC patients, as reported previously (44), and in tissue from mouse models of the disease, *p48-Cre/LSL-KRas^{G12D}* mice (KC mice), which develop extensive PanINs and only invasive carcinoma after age 12 mo (20%), and *p48-Cre/LSL-KRas$^{G12D/+}$/LSL-Trp53$^{R172H/+}$* mice (KPC mice), which develop invasive carcinomas and widespread metastases (45). Epithelial activation of p110α cooperates with oncogenic KRAS to promote invasive carcinomas in mice. Similarly, neoplastic mouse models harboring global p110γ deficiency (KC/p110γ$^{+/-}$ and KC/p110γ$^{-/-}$, and similar EL-Kras or EK cohorts) exhibited a substantial reduction in tumor burden, corroborating earlier reports (30). Taken together, these observations strengthen the argument for the use of drugs targeting p110γ in the clinic.

Nonetheless, our present results show that under certain condition of excessive nutrients (specifically HFDs), the protective effect of p110γ deficiency was lost. When administered an HFD enriched in ω-6 fatty acids, KC/p110γ$^{+/-}$ and KC/p110γ$^{-/-}$ mice (and similarly in EK cohorts) were histologically indistinct from age-matched KC and EK controls and retained pathological activation of the AKT pathway, likely due to compensation through other p110 isoforms, particularly p110α. Substantial evidence indicates that PI3K plays an important role in setting the balance between nutrient storage and nutrient consumption. KC/p110γ$^{+/-}$ and KC/p110γ$^{-/-}$ mice receiving the HFD developed severe NAFLD along with fibrosis and hyperlipidemia, accompanied by severe metabolic dysfunction and increased lipogenesis. Nonhematopoietic p110γ inhibition had previously been suggested to protect against diet-induced steatosis (12), which we were able to corroborate in our cohort of non–tumor-bearing animals. In this paper, we focused on the setting of PDAC. Thus, a likely explanation for the discrepancy between nontumor and Kras-mutated animals is the well-documented decline in pancreatic exocrine and endocrine function in PDAC (46). Interestingly, low serum amylase levels are associated with NAFLD, apparently independent of comorbid conditions including diabetes, metabolic syndrome, and obesity (47, 48). These observations suggest a potential link between failure of the exocrine pancreas and NAFLD development, a relationship that has remained largely unexplored. Together with the presence of Kras mutations, our phenotype also may represent the adaptation to prolonged exposure of excess lipids, as our mice were kept on the HFD for 35 wk, compared with the 12 wk of the previous study (12).

We acknowledge some limitations of our study, particularly the metabolic phenotyping of liver; its dramatic injury was an incidental result that was not completely considered for the methodologic approach. Further confirmation and expansion of metabolic effects using more rigorous approaches may be needed, with consideration to potential physiological disruptions reported with single housing of mice (49). Additional factors such as animal sex (the previous study used only males) or strain background also need to be considered.

Clinically, NAFLD is the most common abnormality found on liver biopsy (50) and is present in nearly 80% of obese patients (51). While many of these patients have stable or subclinical disease, 20% will progress to nonalcoholic steatohepatitis (NASH). NASH itself is also progressive in nature, and up to 20% of NASH patients will develop cirrhosis (52). These varying liver pathologies are associated with alterations to both Phase I and Phase II drug metabolism (53), which may present significant clinical challenges should they be comorbid with PDAC. For instance, the standard of care drug, gemcitabine, is metabolized by the CYP450 system, and accumulates in the liver following both oral and i.v. dosing (54). Should PDAC patients develop NAFLD in response to a p110γ inhibitor or have existing NAFLD worsened by p110γ inhibition, this may lead to either increased gemcitabine–induced hepatotoxicity, or the buildup of toxic metabolites and the need for drastic dose adjustment in the clinic. Given these potential adverse effects, the mechanisms underlying the observed hepatic toxicity warrant further study. Clinical data suggests that NAFLD is both a risk for and prognostic marker of PDAC (55), and the two can be comorbid given the association between PDAC and obesity (56). PI3K signaling is strongly implicated in NAFLD development, as deletion of PTEN promotes the development of steatosis and insulin hypersensitivity in vivo (57).

This may also be of substantial translational relevance, as PDAC patients commonly develop various types of malabsorption and nutritional deficits due to a decline in pancreas exocrine function (58). In many cases, this decline corresponds to reduced pancreatic lipase activity which often can be found at 5–10% of normal levels (46). Due to the subsequent inability to properly metabolize and absorb dietary lipids from the gastrointestinal tract, patients can develop gastrointestinal complications including steatorrhea, lipid-soluble vitamin deficiencies, and severe abdominal discomfort (58). Should p110γ blockade induce or worsen these events in patients with PDAC by altering lipid metabolism, this may precipitate not only severe drug interactions or toxicities, but also nonadherence to or withdrawal from therapy. Beyond the management of PDAC, this also presents the issue of a potentially significant interaction between p110γ inhibitors with weight loss medications that inhibit pancreatic lipase, such as Orlistat (59).

Thus, it is essential to further dissect the hepatic and metabolic roles of p110γ before implementing a regimen that includes p110γ inhibitors to treat patients with PDAC. While relatively little is known regarding p110γ itself, PI3K has been shown to control various aspects of metabolism that are commonly altered in PDAC (60). AKT activation has been shown to stimulate aerobic glycolysis with no change in oxygen consumption,

implicating the PI3K pathway in the Warburg effect (61). In fact, in the absence of mitochondrial respiration in lymphoma cells, there were compensatory increases in PI3K/AKT activity (62), potentially explaining activation of this pathway in the hypoxic PDAC microenvironment (63).

Moreover, PI3K signaling appears to regulate glucokinase activity, further underscoring the contributions of the PI3K pathway to metabolic homeostasis in a variety of tissue types (64). Specifically, p110γ is integral to the appropriate β cell insulin response to glucose (65). As metabolic syndrome (a cluster of clinical disorders including obesity, insulin resistance, and dyslipidemia) appears to be linked to both cancer incidence and hepatic dysfunction (66, 67), it is possible that these effects are at least somewhat mediated by the PI3K pathway. This may be particularly true for cancers of the pancreas, in which patients harboring abnormal glucose metabolism have a significantly greater risk of developing this disease (68). PI3K signals also appear to regulate lipid metabolism and biosynthesis. In rat liver cells, the PI3K downstream effector mTORC1 was shown to be required for lipogenesis, yet was dispensable for gluconeogenesis (69). Similarly, Pan-PI3K or mTOR inhibition impaired lipogenesis and fatty acid oxidation in cultured hepatocytes, further substantiating the role of PI3K in maintaining proper lipid balance (70, 12). Progression of PDAC can be caused by dysregulated cytokine status, which might be a major contributor to poor outcome in PDAC patients with NAFLD (35). We observed TNF-α secretion from hepatocytes in response to p110γ knockout in mice fed an HFD. Whether TNF-α represents organ-to-organ cross-talk between pancreas and liver warrants future consideration.

To summarize, our findings suggest careful consideration when implementing a drug regimen that includes p110γ inhibitors in the management of PDAC. Many patients with PDAC already harbor underlying metabolic dysfunction, which may be significant and predictive of exacerbation when using such approaches, especially in obese patients or those who consume diets high in fat. HFDs can nullify the reduction in tumor burden associated with p110γ deficiency via compensatory up-regulation of alternate p110 isoforms (*SI Appendix*, Fig. S9). Although p110γ may be a cell-autonomous tumor promoter, systemic p110γ deficiency in the context of damaged exocrine pancreas can lead to moderate hepatotoxicity that becomes severe in the setting of an HFD. Taken together, these observations suggest that drugs targeting the PI3K pathway may have limited use in the management of PDAC and may introduce an increased risk for adverse effects, including NAFLD, particularly in the setting of obesity. Further research is needed to identify the factors that mediate the interaction between the pancreas and liver and the possible role of adipose tissue in this system.

Materials and Methods

Mice. PI3Kγ$^{-/-}$ mice (global loss) were described previously (71, 72) and generously provided by Emilio Hirsh. PI3KCA (conditional allele, dependent on Cre expression) mice also were described previously (73) and were obtained from The Jackson Laboratory. These animals were crossed to p48-Cre/LSL-Kras^{G12D} (KC) to generate p48-Cre/LSL-p110α^{CA}, KC/p110γ$^{+/-}$, and KC/p110γ$^{-/-}$ mice, all in the C57/B6 background at an approximate 50:50 male:female ratio. The Elastase-KRAS^{G12D} (EK) mouse model was also used, and we likewise obtained EK/p110γ$^{+/-}$ and EK/p110γ$^{-/-}$ mice. Males and females were included in the study. All the animals were killed at age 9–10 mo except for the p48-Cre/LSL-KRAS^{G12D}/LSL-TP53^{R163H} (KPC) mice, which were killed at 4 mo. Mice were killed using ketamine/xylazine (100/10 mg/kg) until unresponsive to toe tap and/or agonal breathing, after which blood was collected using cardiac puncture. Thoracotomy served as the primary form of killing, and exsanguination was the secondary form. Animals of the genotypes in question were selected at random to reach the desired number after being evaluated. No animals of the desired genotype were excluded from any group, and no further randomization was used. All mice were housed under a 12-h light/12-h dark cycle and had free access to sterile water and pellet food (chow or diet) ad libitum (including the HFD). The animal care and experimental procedures were approved by the Animal Care Committee of the University of Illinois at Chicago. The mice were compared with age-matched WT and non–tumor-bearing mice (p110γ$^{+/-}$ and p110γ$^{-/-}$) also fed on a standard ND and an HFD. More details of the study methodology are provided in *SI Appendix*.

ACKNOWLEDGMENTS. This work was supported by National Cancer Institute Grant CA161283 and University of Illinois at Chicago Departmental Funds (to P.J.G.), and by National Cancer Institute Grants CA 176846 and CA 216410 and Veterans Administration Merit Award BX002703 (to A.R.).

1. R. L. Siegel, K. D. Miller, A. Jemal, Cancer statistics, 2017. *CA Cancer J. Clin.* **67**, 7–30 (2017).
2. Z. Wang *et al.*, Pancreatic cancer: Understanding and overcoming chemoresistance. *Nat. Rev. Gastroenterol. Hepatol.* **8**, 27–33 (2011).
3. M. Gnanamony, C. S. Gondi, Chemoresistance in pancreatic cancer: Emerging concepts. *Oncol. Lett.* **13**, 2507–2513 (2017).
4. D. Zeitouni, Y. Pylayeva-Gupta, C. J. Der, K. L. Bryant, KRAS mutant pancreatic cancer: No lone path to an effective treatment. *Cancers (Basel)* **8**, E45 (2016).
5. S. Eser, A. Schnieke, G. Schneider, D. Saur, Oncogenic KRAS signalling in pancreatic cancer. *Br. J. Cancer* **111**, 817–822 (2014).
6. E. A. Collisson *et al.*, A central role for RAF→MEK→ERK signaling in the genesis of pancreatic ductal adenocarcinoma. *Cancer Discov.* **2**, 685–693 (2012).
7. K. H. Lim, C. M. Counter, Reduction in the requirement of oncogenic Ras signaling to activation of PI3K/AKT pathway during tumor maintenance. *Cancer Cell* **8**, 381–392 (2005).
8. Y. Samuels *et al.*, High frequency of mutations of the PIK3CA gene in human cancers. *Science* **304**, 554 (2004).
9. E. Castellano, J. Downward, RAS interaction with PI3K: More than just another effector pathway. *Genes Cancer* **2**, 261–274 (2011).
10. B. Vanhaesebroeck, L. Stephens, P. Hawkins, PI3K signalling: The path to discovery and understanding. *Nat. Rev. Mol. Cell Biol.* **13**, 195–203 (2012).
11. M. A. Whitehead, M. Bombardieri, C. Pitzalis, B. Vanhaesebroeck, Isoform-selective induction of human p110δ PI3K expression by TNFα: Identification of a new and inducible PIK3CD promoter. *Biochem. J.* **443**, 857–867 (2012).
12. B. Becattini *et al.*, PI3Kγ within a nonhematopoietic cell type negatively regulates diet-induced thermogenesis and promotes obesity and insulin resistance. *Proc. Natl. Acad. Sci. U.S.A.* **108**, E854–E863 (2011).
13. L. X. Li *et al.*, Role of phosphatidylinositol 3-kinasegamma in the β-cell: Interactions with glucagon-like peptide-1. *Endocrinology* **147**, 3318–3325 (2006).
14. P. E. MacDonald *et al.*, Impaired glucose-stimulated insulin secretion, enhanced intraperitoneal insulin tolerance, and increased β-cell mass in mice lacking the p110γ isoform of phosphoinositide 3-kinase. *Endocrinology* **145**, 4078–4083 (2004).
15. E. E. Stratikopoulos, R. E. Parsons, Molecular pathways: Targeting the PI3K pathway in cancer-BET inhibitors to the rescue. *Clin. Cancer Res.* **22**, 2605–2610 (2016).
16. R. Fritsch *et al.*, RAS and RHO families of GTPases directly regulate distinct phosphoinositide 3-kinase isoforms. *Cell* **153**, 1050–1063 (2013).
17. S. Eser *et al.*, Selective requirement of PI3K/PDK1 signaling for Kras oncogene-driven pancreatic cell plasticity and cancer. *Cancer Cell* **23**, 406–420 (2013).
18. S. Yamamoto *et al.*, Prognostic significance of activated Akt expression in pancreatic ductal adenocarcinoma. *Clin. Cancer Res.* **10**, 2846–2850 (2004).
19. Y. Mao *et al.*, Combination of PI3K/Akt pathway inhibition and Plk1 depletion can enhance chemosensitivity to gemcitabine in pancreatic carcinoma. *Transl. Oncol.* **11**, 852–863 (2018).
20. B. Vanhaesebroeck, J. Guillermet-Guibert, M. Graupera, B. Bilanges, The emerging mechanisms of isoform-specific PI3K signalling. *Nat. Rev. Mol. Cell Biol.* **11**, 329–341 (2010).
21. C. Gonella *et al.*, The p110beta isoform of phosphoinositide 3-kinase signals downstream of G protein-coupled receptors and is functionally redundant with p110gamma. *Proc. Natl. Acad. Sci. U.S.A.* **105**, 8292–8297 (2008).
22. D. G. Winkler *et al.*, PI3K-δ and PI3K-γ inhibition by IPI-145 abrogates immune responses and suppresses activity in autoimmune and inflammatory disease models. *Chem. Biol.* **20**, 1364–1374 (2013).
23. T. M. Randis, K. D. Puri, H. Zhou, T. G. Diacovo, Role of PI3Kdelta and PI3Kgamma in inflammatory arthritis and tissue localization of neutrophils. *Eur. J. Immunol.* **38**, 1215–1224 (2008).
24. M. M. Kaneda *et al.*, PI3Kγ is a molecular switch that controls immune suppression. *Nature* **539**, 437–442 (2016).
25. P. Liu, H. Cheng, T. M. Roberts, J. J. Zhao, Targeting the phosphoinositide 3-kinase pathway in cancer. *Nat. Rev. Drug Discov.* **8**, 627–644 (2009).
26. M. C. Schmid *et al.*, PI3-kinase γ promotes Rap1a-mediated activation of myeloid cell integrin α4β1, leading to tumor inflammation and growth. *PLoS One* **8**, e60226 (2013).
27. T. Sasaki *et al.*, Function of PI3Kγ in thymocyte development, T cell activation, and neutrophil migration. *Science* **287**, 1040–1046 (2000).
28. C. W. Steele, N. A. Kaur Gill, N. B. Jamieson, C. R. Carter, Targeting inflammation in pancreatic cancer: Clinical translation. *World J. Gastrointest. Oncol.* **8**, 380–388 (2016).
29. E. Lupia *et al.*, Ablation of phosphoinositide 3-kinase-gamma reduces the severity of acute pancreatitis. *Am. J. Pathol.* **165**, 2003–2011 (2004).

30. M. M. Kaneda *et al*., Macrophage PI3Kgamma drives pancreatic ductal adenocarcinoma progression. *Cancer Discov.* **6**, 870–885 (2016).
31. L. M. Knab, P. J. Grippo, D. J. Bentrem, Involvement of eicosanoids in the pathogenesis of pancreatic cancer: The roles of cyclooxygenase-2 and 5-lipoxygenase. *World J. Gastroenterol.* **20**, 10729–10739 (2014).
32. E. Mascariñas, G. Eibl, P. J. Grippo, Evaluating dietary compounds in pancreatic cancer modeling systems. *Methods Mol. Biol.* **980**, 225–248 (2013).
33. E. C. Cheon *et al*., Alteration of strain background and a high omega-6 fat diet induces earlier onset of pancreatic neoplasia in EL-Kras transgenic mice. *Int. J. Cancer* **128**, 2783–2792 (2011).
34. Y. Ding *et al*., Omega-3 fatty acids prevent early pancreatic carcinogenesis via repression of the AKT pathway. *Nutrients* **10**, E1289 (2018).
35. Q. Hu, A. Klippel, A. J. Muslin, W. J. Fantl, L. T. Williams, Ras-dependent induction of cellular responses by constitutively active phosphatidylinositol-3 kinase. *Science* **268**, 100–102 (1995).
36. L. M. Thorpe, H. Yuzugullu, J. J. Zhao, PI3K in cancer: Divergent roles of isoforms, modes of activation and therapeutic targeting. *Nat. Rev. Cancer* **15**, 7–24 (2015).
37. J. J. Zhao *et al*., The oncogenic properties of mutant p110α and p110β phosphatidylinositol 3-kinases in human mammary epithelial cells. *Proc. Natl. Acad. Sci. U.S.A.* **102**, 18443–18448 (2005).
38. S. Kang, A. G. Bader, P. K. Vogt, Phosphatidylinositol 3-kinase mutations identified in human cancer are oncogenic. *Proc. Natl. Acad. Sci. U.S.A.* **102**, 802–807 (2005).
39. M. Camps *et al*., Blockade of PI3Kgamma suppresses joint inflammation and damage in mouse models of rheumatoid arthritis. *Nat. Med.* **11**, 936–943 (2005).
40. A. Huang *et al*., Single-agent activity of PIK3CA inhibitor BYL719 in a broad cancer cell line panel, in Proceedings of the 103rd Annual Meeting of the American Association for Cancer Research, March 31–April 4, 2012, Chicago, IL. *Cancer Res.* **72** (Suppl) (2012).
41. S. Kim *et al*., Role of phosphoinositide 3-kinase beta in glycoprotein VI-mediated Akt activation in platelets. *J. Biol. Chem.* **284**, 33763–33772 (2009).
42. R. Lemstrova *et al*., Dysregulation of KRAS signaling in pancreatic cancer is not associated with *KRAS* mutations and outcome. *Oncol. Lett.* **14**, 5980–5988 (2017).
43. E. Lupia, L. Pigozzi, A. Goffi, E. Hirsch, G. Montrucchio, Role of phosphoinositide 3-kinase in the pathogenesis of acute pancreatitis. *World J. Gastroenterol.* **20**, 15190–15199 (2014).
44. C. E. Edling *et al*., Key role of phosphoinositide 3-kinase class IB in pancreatic cancer. *Clin. Cancer Res.* **16**, 4928–4937 (2010).
45. C. Guerra, M. Barbacid, Genetically engineered mouse models of pancreatic adenocarcinoma. *Mol. Oncol.* **7**, 232–247 (2013).
46. E. P. DiMagno, V. L. W. Go, W. H. J. Summerskill, Relations between pancreatic enzyme outputs and malabsorption in severe pancreatic insufficiency. *N. Engl. J. Med.* **288**, 813–815 (1973).
47. K. Nakajima *et al*., Independent association between low serum amylase and nonalcoholic fatty liver disease in asymptomatic adults: A cross-sectional observational study. *BMJ Open* **3**, e002235 (2013).
48. J. M. Yao *et al*., Serum amylase levels are decreased in Chinese non-alcoholic fatty liver disease patients. *Lipids Health Dis.* **13**, 185 (2014).
49. T. R. Nagy, D. Krzywanski, J. Li, S. Meleth, R. Desmond, Effect of group vs. single housing on phenotypic variance in C57BL/6J mice. *Obes. Res.* **10**, 412–415 (2002).
50. P. Angulo, Nonalcoholic fatty liver disease. *N. Engl. J. Med.* **346**, 1221–1231 (2002).
51. A. J. Sanyal; American Gastroenterological Association, AGA technical review on nonalcoholic fatty liver disease. *Gastroenterology* **123**, 1705–1725 (2002).
52. A. J. McCullough, The clinical features, diagnosis and natural history of nonalcoholic fatty liver disease. *Clin. Liver Dis.* **8**, 521–533, viii (2004).
53. M. D. Merrell, N. J. Cherrington, Drug metabolism alterations in nonalcoholic fatty liver disease. *Drug Metab. Rev.* **43**, 317–334 (2011).
54. S. A. Veltkamp, D. Pluim, O. van Tellingen, J. H. Beijnen, J. H. M. Schellens, Extensive metabolism and hepatic accumulation of gemcitabine after multiple oral and intravenous administration in mice. *Drug Metab. Dispos.* **36**, 1606–1615 (2008).
55. C.-F. Chang *et al*., Exploring the relationship between nonalcoholic fatty liver disease and pancreatic cancer by computed tomographic survey. *Intern. Emerg. Med.* **13**, 191–197 (2018).
56. P. M. Bracci, Obesity and pancreatic cancer: Overview of epidemiologic evidence and biologic mechanisms. *Mol. Carcinog.* **51**, 53–63 (2012).
57. B. Stiles *et al*., Liver-specific deletion of negative regulator Pten results in fatty liver and insulin hypersensitivity [corrected]. *Proc. Natl. Acad. Sci. U.S.A.* **101**, 2082–2087 (2004). Correction in: *Proc. Natl. Acad. Sci. U.S.A.* **101**, 5180 (2004).
58. T. Hackert, K. Schütte, P. Malfertheiner, The pancreas: Causes for malabsorption. *Viszeralmedizin* **30**, 190–197 (2014).
59. R. Guerciolini, Mode of action of orlistat. *Int. J. Obes. Relat. Metab. Disord.* **21** (suppl. 3), S12–S23 (1997).
60. R. M. Perera, N. Birdies, Pancreatic cancer metabolism: Breaking it down to build it back up. *Cancer Discov.* **5**, 1247–1261 (2015).
61. R. L. Elstrom *et al*., Akt stimulates aerobic glycolysis in cancer cells. *Cancer Res.* **64**, 3892–3899 (2004).
62. H. Pelicano *et al*., Mitochondrial respiration defects in cancer cells cause activation of Akt survival pathway through a redox-mediated mechanism. *J. Cell Biol.* **175**, 913–923 (2006).
63. M. Erkan, M. Kurtoglu, J. Kleeff, The role of hypoxia in pancreatic cancer: A potential therapeutic target? *Expert Rev. Gastroenterol. Hepatol.* **10**, 301–316 (2016).
64. B. Maiztegui, C. L. Román, H. C. Barbosa-Sampaio, A. C. Boschero, J. J. Gagliardino, Role of islet glucokinase, glucose metabolism, and insulin pathway in the enhancing effect of islet neogenesis-associated protein on glucose-induced insulin secretion. *Pancreas* **44**, 959–966 (2015).
65. J. Kolic, A. F. Spigelman, A. M. Smith, J. E. Manning Fox, P. E. MacDonald, Insulin secretion induced by glucose-dependent insulinotropic polypeptide requires phosphatidylinositol 3-kinase γ in rodent and human β-cells. *J. Biol. Chem.* **289**, 32109–32120 (2014).
66. K. Esposito, P. Chiodini, A. Colao, A. Lenzi, D. Giugliano, Metabolic syndrome and risk of cancer: A systematic review and meta-analysis. *Diabetes Care* **35**, 2402–2411 (2012).
67. M. H. Rodrigues, A. S. Bruno, J. Nahas-Neto, M. E. S. Santos, E. A. Nahas, Nonalcoholic fatty liver disease and metabolic syndrome in postmenopausal women. *Gynecol. Endocrinol.* **30**, 325–329 (2014).
68. D. Johansen *et al*., Metabolic factors and the risk of pancreatic cancer: A prospective analysis of almost 580,000 men and women in the Metabolic Syndrome and Cancer Project. *Cancer Epidemiol. Biomarkers Prev.* **19**, 2307–2317 (2010).
69. S. Li, M. S. Brown, J. L. Goldstein, Bifurcation of insulin signaling pathway in rat liver: mTORC1 required for stimulation of lipogenesis, but not inhibition of gluconeogenesis. *Proc. Natl. Acad. Sci. U.S.A.* **107**, 3441–3446 (2010).
70. D. D. Liu *et al*., Effects of inhibiting PI3K-Akt-mTOR pathway on lipid metabolism homeostasis in goose primary hepatocytes. *Animal* **10**, 1319–1327 (2016).
71. E. Patrucco *et al*., PI3Kgamma modulates the cardiac response to chronic pressure overload by distinct kinase-dependent and -independent effects. *Cell* **118**, 375–387 (2004).
72. E. Hirsch *et al*., Central role for G protein-coupled phosphoinositide 3-kinase gamma in inflammation. *Science* **287**, 1049–1053 (2000).
73. A. Klippel *et al*., Membrane localization of phosphatidylinositol 3-kinase is sufficient to activate multiple signal-transducing kinase pathways. *Mol. Cell. Biol.* **16**, 4117–4127 (1996).